On the different contributions of flexible elements to the structural noise of refrigeration compressors

A. Ricci[1,2], F. Albertz[1], and L. Bregant[2]

[1]BMW AG, Complete Vehicle Development - Acoustic, Vibration and Sound, Knorrstrasse 147, 81700, Munich, Germany

[2]Università degli Studi di Trieste, Department of Engineering and Architecture, Via Valerio 10, 341237, Trieste, Italy

Abstract

Air conditioning acoustics have become of paramount importance in electric vehicles, where noise from electromechanical components is no longer masked by the presence of the internal combustion engine. In a car HVAC systems, the coolant compressor is one of the most important sources in terms of vibration and noise generation. The paper, the generated structural noise is studied in detail on a prototype installation, and the noise transmission and propagation mechanisms are analyzed and discussed. Through "in situ" measurements and virtual point transformation, the rotor unbalance forces and torque acting within the component are identified. The dynamic properties of the rubber mounts, installed between the compressor and its support, are identified thanks to matrix inversion methods. To assess the quality of the proposed procedure, the synthesized sound pressure level is compared with experimental SPL measurements in different operational conditions. The contributions to the structure borne noise of the installed hoses and mounts are evaluated, ranked and commented.

1 Introduction

Over time, vehicle users have become increasingly demanding with respect to the acoustic quality of cars, expecting always better acoustic comfort performances. This expectation, established in the past for vehicles with internal combustion engines, has remained unchanged, if not increased, in electric vehicles, which are perceived to be quieter than conventional ones. This shared perception seems to be confirmed by the work of Eisele et al. [1], in which it is shown that the sound pressure level (SPL) during a full load in an electric vehicle is 12 dBA lower than in a IC engine powered car in second gear. Yet there are also undesirable acoustic phenomena during a full load in electric vehicles. The disappearance of the internal combustion engine has not only removed the main source of noise and vibration, but also its masking effect of other lesser noises, which are now completely audible. Electric vehicles are very often associated with high-frequency noise, but there are situations in which certain subsystems generate low-frequency noise as well. One of these, is the sub-system comprising the vehicle's air conditioning components and more specifically the refrigerant gas compressor. The purpose of this component is not just to treat

the air in the passenger compartment, but also to control the temperature of the battery pack during various operating conditions.

In the automotive industry, especially for efficiency reasons, the most widely used compressor the scroll type [2], which features reduced vibrations in the gas compression phase. The dynamic behavior of the complete system, however, depends on the positioning of the component within the car and on the chosen isolation strategy, and only recently has become an addressable issue [3],[4],[5].Typical operating conditions for this component occur at low frequencies (10÷150 Hz), where it can be modeled as a rigid body. In these conditions, the internal forces and the forces due to the displacement of the body are transferred to the vehicle's chassis through the mounting elements.

Of the various low-frequency acoustic phenomena to be avoided, booming is one of the best known. This phenomenon, already studied in traditional vehicles, occurs when the excitation force has a frequency close to passenger compartment fluid volume modes [6]. In electric vehicles, the refrigerant gas compressor can excite those, and thus the reason for the present paper.

In this work, through "in-situ" measurements the dynamic forces developed by the compressor are identified. The properties of the insulating mounts, based on nominal values, are optimized thanks to the inertance and the apparent mass matrices of the system. Experimental measurements show that the hoses have a significant influence on the dynamics of the complete system, and also play an important role in the structure-borne noise propagation. The paper describes how to isolate and identify their contribution to SPL, through measurements in a prototype installation.

2 Methods

The procedure is divided in two distinct steps. The first objective is to identify the internal dynamic forces, acting on the supporting structure, during the compressor's operation. This can be done, in the absence of a dedicated test bench, or detailed information on the stiffness and mass-inertia matrix of the system, using inversion techniques. If the component is mounted trough insulating elements and can be considered as decoupled from the rest of the structure, the internal forces can be derived by knowing the apparent mass matrix and the accelerations of the component in operation.

The apparent mass matrix is determined by inverting the experimentally obtained full inertance matrix. Starting from the equation of motion:

$$M\ddot{x} + C\dot{x} + Kx = F_a \tag{1}$$

using the Laplace transform, and making some simplifications neglected here for brevity, can be re-written as:

$$\underbrace{-\omega^2 X}_{\text{acceleration term}} \quad (M + \frac{Cj}{\omega} + \frac{K}{-\omega^2}) = F \tag{2}$$

The term $-\omega^2 X$ (acceleration) is factored out, to obtain the force/acceleration ratio. The terms between brackets represent the Apparent Mass $[AM]$. This can also be represented as a real mass M and a complex frequency dependent stiffness $\underline{K}(\omega)$. In the latter, the real part is a stiffness and the imaginary part a damping.

$$[AM] = \frac{F}{-\omega^2 X} = M + \frac{Cj}{\omega} + \frac{K}{-\omega^2} \tag{3}$$

$$= M + \frac{-Cj\omega + K}{-\omega^2} \tag{4}$$

$$= M + \frac{\underline{K}(\omega)}{-\omega^2} \tag{5}$$

Since the considered phenomenon occurs at low frequency, where the treated component behaves as a rigid body, it is possible to describe the kinematics of the complete compressor through a virtual point (VP). Therefore, thanks to a virtual point transformation [7],[8],[9], based on geometrical considerations, it is possible to reduce the (n-dimensional) system to only 6 DoF of rigid body. Both the inertance and the apparent mass matrix can be computed in this location. The accelerations,

measured under operating conditions, which are discussed in the following section, are also transformed into the same VP. This results in a 6x6 system of equations.

By combining the matrix $[AM]$ with the accelerations in operation, it is possible to determine the dynamic forces under the same conditions.

$$\{F_{dyn,int}\} = [AM] \cdot \{\ddot{x}_{op}\} \tag{6}$$

Inverse methodologies, although successfully applied, present problems due to condition number of the matrix to be inverted. Through an appropriate VP transformation, this difficulties can be reduced. A strategic positioning of the VP, close to the system's centre of mass (or elastic centre, also defined EC, of the system when available [10][11][12]) allows in fact to reduce the magnitude of the off-diagonal elements of the inertance matrix, facilitating the inversion procedure.

By experimentally detecting the inertance matrix [13][14] and the apparent mass matrix, the mass and moment of inertia matrix of a component can also be determined using "in-situ" measurements. These make it possible to correct the system matrices based on first-principles, used in analytical models to simulate the system. In this sense, the dynamic stiffness matrix and the mass and moment of inertia matrices can be optimized so that the difference between the analytical and experimental FRFs, of both the inertia matrix and its inverse, are minimized.

The second objective is the synthesis of the sound pressure in the passenger compartment, at the driver's ear. To this account, the most commonly used tool transfer path analysis (TPA). When it is not possible to use a dedicated test bench for the determination of blocked forces [15][16], classical TPA is used. TPA is a widely accepted tool, and successfully used in many industrial sectors. In the automotive industry it is frequently used when dealing with vibro-acoustic problems[17]. Especially when, as in this case, the component can be easily extracted from the vehicle, the most convenient methodology is classical TPA[18].

When dealing with low-frequency structural noise, air-borne noise contributions can be neglected, [19], reducing the synthesis to:

$$SPL_d(\omega) = \sum_j Y_{dj}(\omega) \cdot f_j \tag{7}$$

where:

- SPL_d is the resulting sound pressure level at the driver's ear
- Y_{dj} represents the generic impedance matrix of structure borne transfer functions between a j^{th} position at the sub-frame and the driver's ear
- f_j are the forces transmitted from the active component to the passive component along the j^{th} path

The final step is to perform a complete synthesis of the SPL due to the dynamic excitations that the compressor applies to the support frame. The synthesis is validated through in-vehicle SPL measurements under the same conditions.

The real mounts' dynamic stiffnesses are unknown, and as they are very low ($K_{stat} < 40\frac{N}{mm}$) it is particular demanding to make dynamic component test bench measurements. For the determination of the dynamic forces acting between source and receiver, a dynamic stiffness model is used. Starting from the static stiffness values of the supports, dedicated functions are used to model the stiffening gain factor. The modelled dynamic stiffnesses are then verified by means of experimental measurements, and updated from these.

2.1 Data acquisition

The compressor analysed in this paper is highlighted in red in figure 4. This is mounted, on the car frame mock-up, using three identical rubber mounts. The installation is prototypical, and it is mainly used for compressor identification and structure isolation studies. On the right side of the figure there are heat exchangers. The latter are connected to the compressor by two pipes, a suction hose and a pressure hose, which, for sake of clarity, are not included in the CAD drawing.

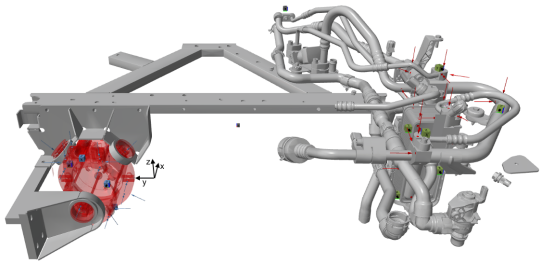

Figure 1: Representation of the system. The refrigerant compressor is highlighted in red. It is attached to the front chassis side utilizing a prototypical sub-frame. The mounting strategy is based on a single level of decoupling.

(a) Without the hoses (b) With operational hoses installed

(c) With extra-long hoses

Figure 2: Configurations in which compressor characteristics can be identified.

The system can be identified under three different conditions, represented schematically in figure 2.

Since no information is available with respect to the dynamic characteristics of the hoses, the inertance matrix of the system is identified without those elements, as shown in figure 2a. In this configuration the system under identification consists of the compressor and its mounts only. The required measurements are performed via rowing hammer excitation,using six tri-axial accelerometers for the responses. The carefully positioned response points and the number of excitation locations are chosen to yield to an over-determined system of equations, in order to reduce the mentioned inversion inaccuracies figure 4. The measured inertance matrix is than condensed into the selected VP. The resulting matrix is 6x6, with non-zero off diagonal elements, representing the coupled dynamic of the compressor.

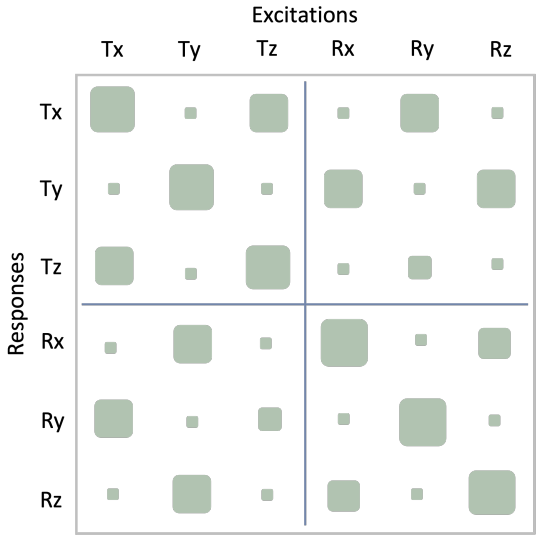

Figure 3: Inertance Matrix for the electric compressor measured in-situ for the 6DoF of the virtual point-V P . The squares in the figure represent the response of each individual degree of freedom, to a unit excitation in each of them

The magnitude of the off diagonal elements is minimized with the proper definition of the VP. Since this doesn't coincide with the EC of the system, coupled phenomena still exists. As for example in the upper-left matrix, where a force applied in the X direction produces relevant displacement also in Z.

To the SPL synthesis also the operational accelerations of the working compressor are needed. These are acquired in two different configurations. In the first one, visible in figure 2b, while using the real hoses. The second one, shown in the figure 2c , with extra-long hoses with the aim to minimize their loads transferring capabilities. These are much longer and more flexible than the operational ones, with inertial masses applied to them. The proposed

configuration minimize the hoses movements during the compressor's operation.

In both the adopted configurations, the accelerations measured by each sensors are synthesised in the virtual point VP [7], in the same way as for the inertance matrix.

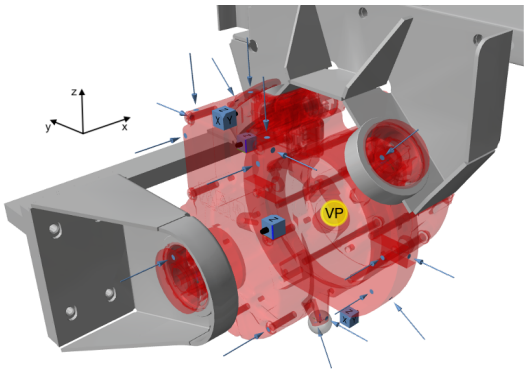

Figure 4: Representation of the system. Accelerometers points and excitations direction are highlighted, as well as the chosen VP.

The compressor is then dismounted from the frame, allowing for the noise transfer functions (NTFs) measurements. Each constraint point is independently identified using, again, VP theory. For each interface point, three triaxial accelerometers and a suitable number of excitations are used, in line with what has been previously described. A VP is positioned, as visible in the figure 5, in the corresponding mount's elastic centre, which lies in the centre of the interface point.

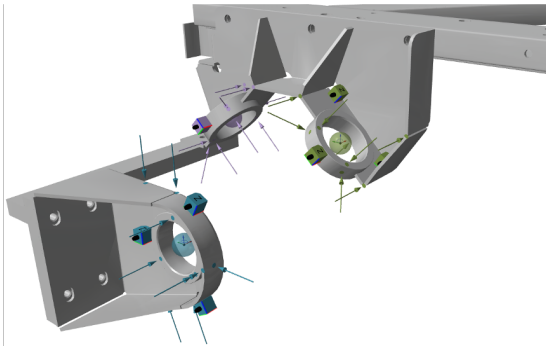

Figure 5: Measurement campaign for the acquisition of the noise transfer functions from the compressor holder to the driver's ears.

The measurements under operating conditions, necessary both for the determination of the dynamic forces and for the SPL synthesis, are performed keeping the accelerometers positioned on the compressor as in the figure 4. To identify the system properties, a pressure sweep, from 7 to 14 bar, is used. This encompasses, the rotation compressor's frequency range $10 \div 150$ Hz, where the major contribution, come from the first order of rotation harmonic.

The data acquisition is performed using an MKII system from Müller-BBM, while the preprocessing is done in PAK suite. Since, the excitations relate mainly to the first order of rotation, a dedicated order analysis, according to an internal standardized procedure is performed. This is done for all measured quantities, i.e. accelerations and forces.

Starting from the accelerations, integrating those twice and using the mentioned kinematic relations, it is possible to synthesise the displacements of the compressor, under operating condition within each mount.[7].

3 Results

When dealing with matrix inversion, it's possible to run into ill-conditioned problems; this condition is highlighted by the condition number of the matrix that needs to be inverted. Figure 6 shows the condition number as a frequency function of the VP-inertance matrix.

With an high condition number, the inversion is sensitive to any measurement errors, in this case especially at low frequencies, up to 50 Hz. The condition number, then, decreases to values close to 450, and then remains constant.

Unfortunately for the specific problem, the most interesting range is between $10 \div 30$Hz where the most of the dynamics of the compressor appears. In here the aim is to minimize the difference between the analytical and the experimental results, using the information contained in the elements of the inertance and the apparent mass matrices.

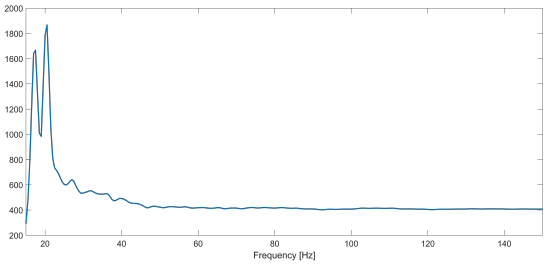

Figure 6: Condition number of the inertance matrix as function of frequency.

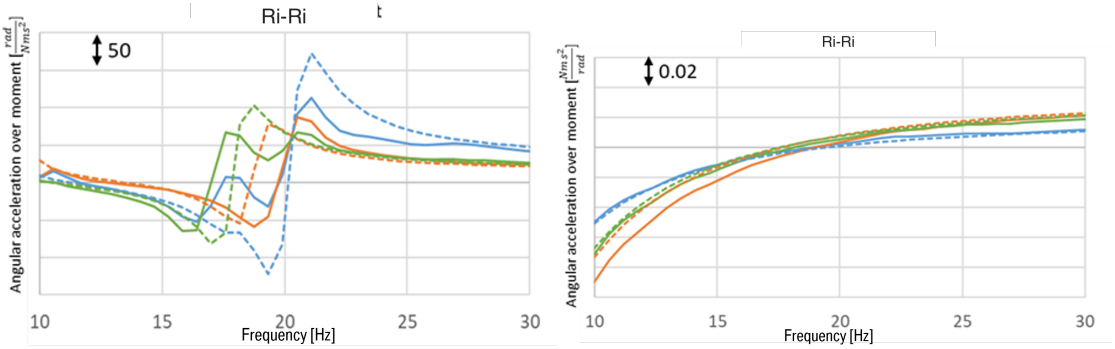

(a) Inertance - Real Component

(b) Apparent Mass - Real Component

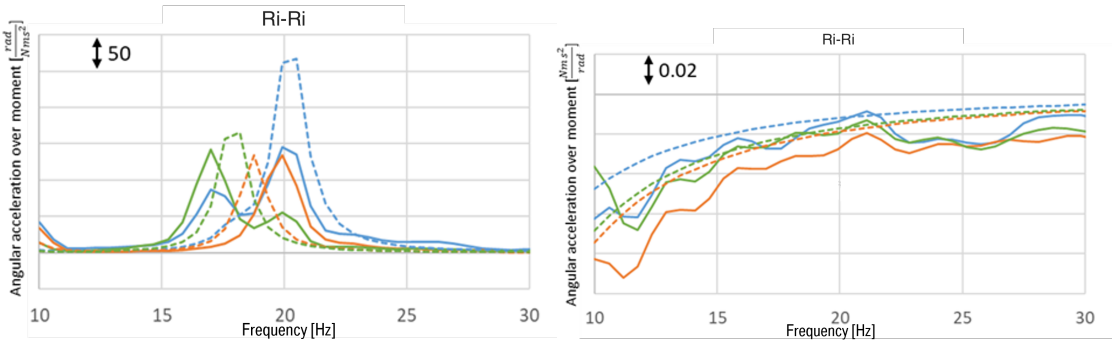

(c) Inertance - Imaginary Component

(d) Apparent Mass - Imaginary Component

Figure 7: Comparison of the simulated (- - - -) and experimentally determined FRFs (——), both in the inertance and apparent mass FRF Matrix prior the optimization of the system matrices optimization; Rx-Rx ——; Ry-Ry ——; Rz-Rz ——

With reference to figure 3, some results will be highlighted; for sake of brevity non all the matrices' elements will be displayed and discussed, but the general behaviour is common to all of them. The first proposed comparison regards the main diagonal FRF elements of the lower right sub-matrix where the rotational Ri DoF are stored. The comparison between ana-

lytical and experimental data is visible in figure 3. It can be observed that while the inertance FRF (9a and 9c) do show discrepancies, the apparent mass FRF (9b and 9d)denote an better match to each other. The system inversion appears to be less error sensitive, and therefore the inverted data are in line with the analytical ones.

The influence of the flexible modes of the receiving structure has a negligible influence on the FRFs of the mounted system. As previously written, the first flexible modes occur at frequencies far away from the studied frequency range. The observed differences are therefore depending from the initial parameters' values used in the simulation of the system. These will need to be updated in order to generate FRFs closer to the experimentally measured ones.

The second group to be considered, are the off diagonal FRFs belonging to the upper left-sub matrix, translation Ti-Tj DoF. Those elements display the coupled effects due to the positioning of the rubber mounts. As previously said for the Ri-Ri DoF, also in this case the inertance FRFs shows the need to update the analytical model parameters. The apparent mass FRFs (10b and 10d respectively) should be a constant value (as the dashed lines). The plots show that the correlation between numerical and experimental results is not very high.

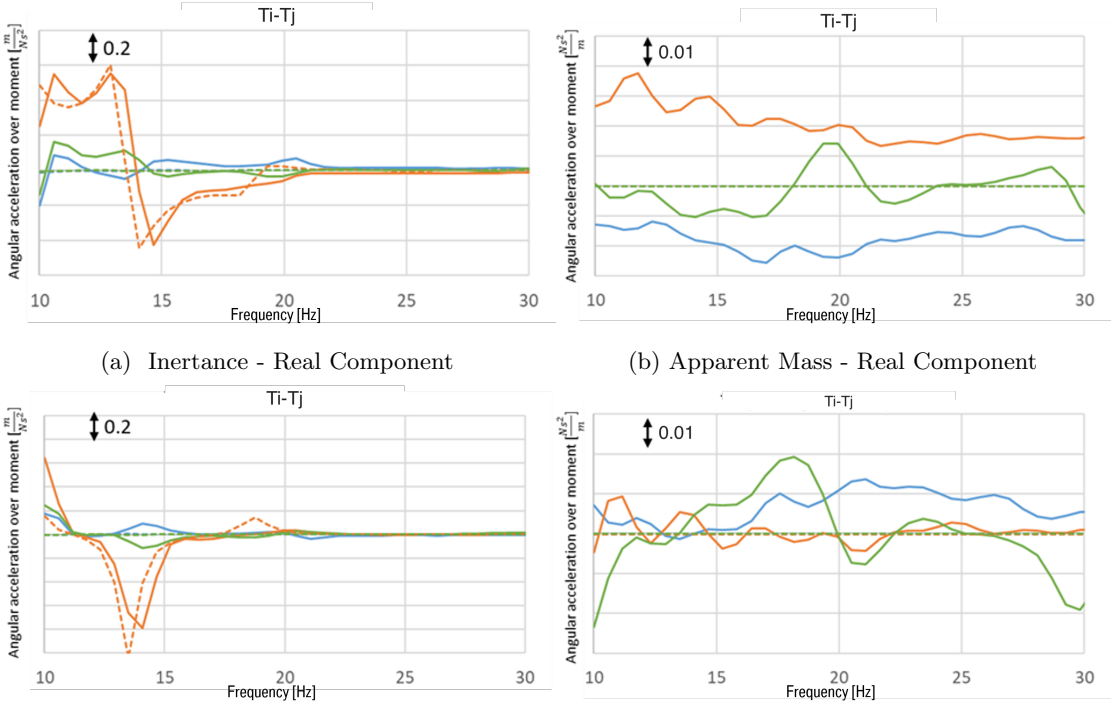

(a) Inertance - Real Component

(b) Apparent Mass - Real Component

(c) Inertance - Imaginary Component

(d) Apparent Mass - Imaginary Component

Figure 8: Comparison of the simulated (- - - -) and experimentally determined FRFs (——), both in the inertance and apparent mass FRF Matrix; Tx-Ty ——; Tx-Tz ——; Ty-Tz ——

To improve the match between the FRFs families, both the inertance and the apparent mass FRFs, the analytical model parameters will be updated on the base of the experimental results. Both the inertia and the dynamic stiffness system's matrices are updated. The parameters of these two are varied within limits considered to be physical, still to obtain re-

alistic solutions. The inertia matrix of the system can be determined within few percentage points, while the variations of the dynamic stiffness can be much higher. As a matter of fact, nominally identical mounts can exhibit differences up to 15%, in each direction, due to manufacturing and material tolerances. The exact starting values, the ranges of variation and the final results of the updating process will not be given in detail, for company policies.

On the base of multi-objective optimisation, the system parameters were updated, in order to minimise the error between numerical and experimental FRFs, simultaneously for both inertance and apparent mass FRFs. Since the initial guess values and the final solution ones, are not too far apart, it was decided to use a General Reduced Gradient (GRD) algorithm.

The results provided by the optimisation are visible in 9 and 10.

The model updating has considerably improved the match of the rotational DoF-FRFs of the inertance matrix, based on a on purposed developed correlation index. At the same time, the apparent mass FRFs are showing an improved correlation even if this was already good before the updating process.

Similarly for the Ti-Tj FRFs, the updating significantly improves the inertance FRF correlation(10a and 10c) and also the corresponding inverse curves present a better numerical experimental results match .

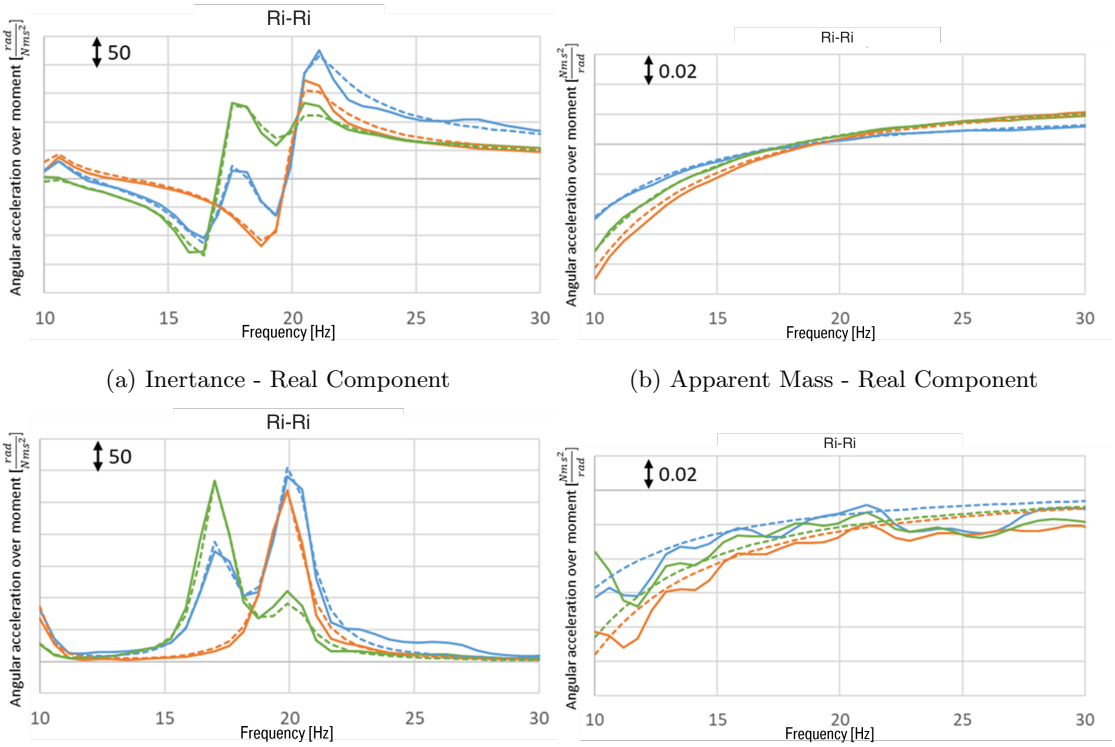

(a) Inertance - Real Component

(b) Apparent Mass - Real Component

(c) Inertance - Imaginary Component

(d) Apparent Mass - Imaginary Component

Figure 9: Comparison of the simulated (- - - -) and experimentally determined FRFs (——), both in the inertance and apparent mass FRF Matrix; Rx-Rx ——; Ry-Ry ——; Rz-Rz ——

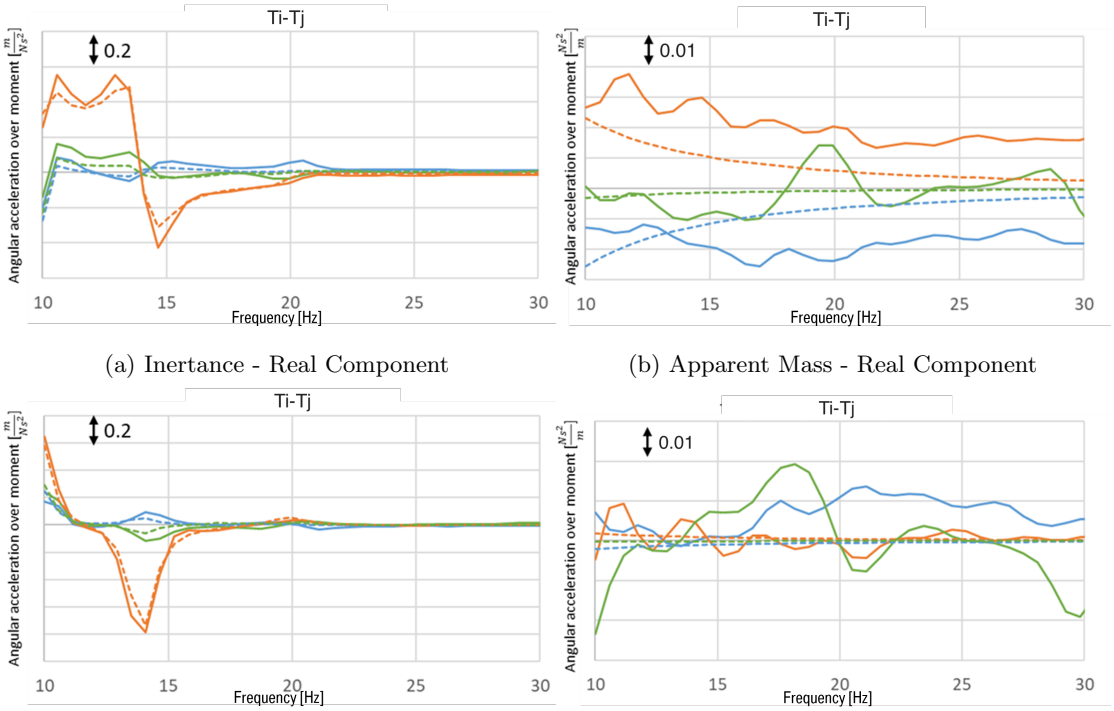

(a) Inertance - Real Component

(b) Apparent Mass - Real Component

(c) Inertance - Imaginary Component

(d) Apparent Mass - Imaginary Component

Figure 10: Comparison of the simulated (- - - -) and experimentally determined FRFs (——), both in the inertance and apparent mass FRF Matrix
Tx-Ty ——; Tx-Tz ——; Ty-Tz ——

After the determination of the system apparent mass matrix, is it possible, according to equation 6 to identify the internal dynamic forces generated by the compressor. For this study, the inertance FRFs are combined with the operational accelerations in different operating conditions, once utilizing the normal hoses and once utilizing the extra-long hoses (respectively figure 2b and figure 2b).

The comparison of the generated forces, in the two configurations is visible in figure 11, where those are depicted in the three main directions x, y and z. The x force values represent the gas compression, while y and z ones represent the unbalance of the compressor's rotor, which should, in principle, be identical.

The discrepancies among the curves, around 110Hz, surely depends from the different contribution of the hoses' dynamic stiffness to the assembly behaviour, remaining all the rest equal for the two operation tests.

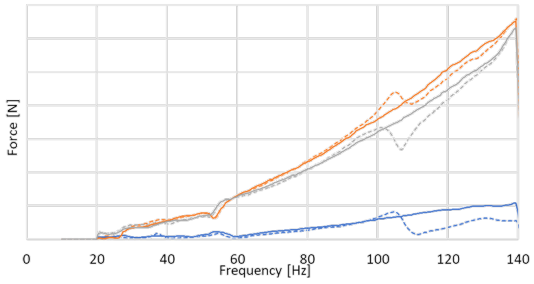

Figure 11: ——Force without the hoses' influence ; - - - -Force including the hoses' influence. ——Force in x direction.——Force y direction. ——Force in z direction.

The requested last step is the SPL synthesis. The dynamic forces, acting at each mount location are obtained combining the mount's

dynamic stiffness and the displacements in each mount's VP, as described in figure 5. Similarly to what has been done for the identification of the forces, the contribution of the hoses to the SPL is evaluated considering in two different piping configurations (standard - extra long), to validate their contribution to the structure borne noise.

The results of the SPL synthesis are displayed in figure 12. The synthesis of the SPL excluding the hoses' contributions is compared to the SPL measurements in the same configuration (blue orange curves), The agreement is definitively satisfactory. The analysis are shown here between $20 \div 140$ Hz. In the range 25-35 Hz, the simulated results differ some more from the measured ones, due to the presence of rigid body modes of the compressor, which occur precisely in this frequency band

Figure 12: SPL perceived at the driver's ear
——Measured SPL with isolated hoses
——Synthetized SPL isolating the hoses
——Measured SPL including the hoses contribution

The SPL measured utilizing normal hoses is now compared with the previous results, this value is represented by the red line figure 12).

It can be seen that at low frequencies, i.e. up to 80 Hz, the contribution of the hoses is not apparent. For frequencies between $90 \div 140$ Hz, the contribution of the hoses leads to an increase in SPL between 5 and 10 dBA. It can be seen that the hoses have a detectable contribution to the structural noise generated by the compressor. The latter derives from the dynamic stiffness of the hoses themselves and influences in a not negligible way the SPL after 80 Hz.

4 Conclusions

In this work a refrigerant compressor has been analyzed regarding both the internally generated forces and the low frequency structure borne noise perceived at the drivers' ears.

"In-situ" methodologies, which includes inverse techniques, have been successfully applied for the identification of the system's apparent mass. The limitation of this methodology has been described in relation to the coupled elements of the inertance matrix, which are heavily affected by the matrix condition number. This is not the case for the elements populating the main diagonal that are less sensible to measurements errors. Through an optimization step it is possible to improve the quality of the inertance FRFs, while the apparent mass FRFs are less sensitive to this process.

The identification of the internally generated dynamic forces has demonstrated how the hoses do not only represent structure borne noise paths, but also affect the global dynamic stiffness of the compressor-supporting frame system. All these contributions need to be included in numerical model when simulating the hosed systems.

The classical TPA methodology has been validated using measured data. This study has allowed to identify and quantify the contribution, to the booming noise, deriving from the hoses. In the frequency range $90 \div 140$ Hz, this participation is roughly between 5 and 10 dB, showing the importance of including the hoses dynamics in the analysis of the complete system.

References

[1] G. Eisele, K. Wolff, P. Genender, and G. J. Schürmann, "Electric vehicle sound design - just wishful thinking?" in *Proceedings of Aachen acoustic colloquium*, November 2010.

[2] J. Aurich and R. Baumgart, "Comparison and evaluation of different a/c compressor concepts for electric vehicles," *International Compressor Engineering Conference*, pp. 1433–1443, 2018.

[3] S. Bennouna, T. Matharan, and O. Cherlaux, "Automotive hvac noise reduction," *SAE Technical Paper*, 2018.

[4] M. Häussler, D. Kobus, and D. J. Rixen, "Parametric design optimization of e-compressor nvh using blocked forces and substructuring," *Mechanical System and Signal Processing*, vol. 150, 2021.

[5] S. T. Lim, K. H. Joo, H. N. Ahn, Y. D. Park, and Y. J. Kang, "Transfer characteristics of vehicle air conditioners' booming noise," *Journal of Mechanical Science and Technology*, vol. 28, no. 6, pp. 2025–2031, 2014.

[6] G. Cerrato, "Automotive sound quality – powertrain, road and wind noise," *Sound and Vibration*, pp. 16–24, 2009.

[7] A. Ricci, F. Albertz, and L. Bregant, "Data-based powertrain mounts characterization for driveline booming predictions utilizing virtual sensing," in *Proceedings of ISMA2020*, 2020.

[8] M. V. der Seijs, "Experimental dynamic substructuring: Analysis and design strategies for vehicles development," Ph.D. dissertation, Delft University of Technology, 2016.

[9] M. Häussler, "Modular sound and vibration engineering by substructuring," Ph.D. dissertation, Technische Universität München, 2021.

[10] D. E. Whitney and J. M. Rourke, "Mechanical behavior and design equations for elastomer shear pad remote center compliances," *Jorunal of Dynamic Systems, Measurements, and Control*, vol. 108, pp. 223–232, 1986.

[11] N. Ciblak and H. Lipkin, "Design and analysis of remote center of compliance structures," *Journal of Robotic Systems*, vol. 20, no. 8, pp. 415–427, 2003.

[12] S. Joo, H. Waki, and F. Miyazaki, "On the mechanics of elastomer shear pads for remote center compliance (rcc)," *Proceedings of the 1996 IEEE International Conference on Robotics and Automation*, pp. 291–298, 1996.

[13] A. Fregolent and A. Sestieri, "Identification of rigid body inertia properties from experimental data," *Mechanical System and Signal Processing*, vol. 10, no. 6, pp. 697–709, 1996.

[14] O. Vahid, A. Khajepour, F. Ismail, and C. R. Urbaniak, "In situ identification of vehicle engine inertia properties," *Int. J. Vehicle Noise and Vibration*, vol. 3, no. 1, pp. 46–69, 2007.

[15] D. Lennström, M. Olsson, F. Wullens, and A. Nykänen, "Validation of the blocked force method for various boundary conditions for automotive source characterization," *Applied Acoustic*, vol. 102, pp. 108–119, 2016.

[16] T. Gras, O. Aubry, A. Menon, and J. Champain, "Blocked forces characterization of an air-conditioning compressor – application to the norm iso-21955," *inter.noise 2019 Noise Control for a Better Environment*, 2019.

[17] J. Plunt, "Finding and fixing vehicle nvh problems with transfer path analysis," *Sound and Vibration*, pp. 12–16, 2005.

[18] M. V. van der Seijs, D. de Klerk, and D. J. Rixen, "General framework for transfer path analysis: History, theory and classification of techniques," *Mechanical System and Signal Processing*, vol. 68, no. 69, pp. 217–244, 2016.

[19] A. Cloix, H. Siwiak, P. Bouvet, F. Barillon, and P. Mordillat, "Characterisation of the booming noise variability in a vehicle," *Proceeding of ISMA 2021-USD2012*, pp. 4513–4524, 2012.